Published in final edited form as:
Circ Arrhythm Electrophysiol. 2011 June ; 4(3): 279–286. doi:10.1161/CIRCEP.110.960567.

Gaps in the Ablation Line as a Potential Cause of Recovery from Electrical Isolation and their Visualization using MRI

Ravi Ranjan, MD, PhD,
Departments of Medicine/Cardiology, University of Utah, Salt Lake City, UT 84132

Ritsushi Kato, MD, **Menekhem M. Zviman, PhD**,
Department of Medicine/Cardiology, Johns Hopkins Hospital, Baltimore, MD.

Timm M. Dickfeld, MD,
Departments of Medicine/Cardiology, University of Maryland, Baltimore, MD.

Ariel Roguin, MD,
Departments of Medicine Rambam Medical Center, Rappaport Faculty of Medicine, Haifa, Israel.

Ronald D. Berger, MD, PhD,
Department of Medicine/Cardiology, Johns Hopkins Hospital, Baltimore, MD; Department of Biomedical Engineering, Johns Hopkins Hospital, Baltimore, MD.

Gordon F. Tomaselli, MD, and
Department of Medicine/Cardiology, Johns Hopkins Hospital, Baltimore, MD.

Henry R. Halperin, MD, MA
Department of Medicine/Cardiology, Johns Hopkins Hospital, Baltimore, MD; Department of Radiology, Johns Hopkins Hospital, Baltimore, MD; Department of Biomedical Engineering, Johns Hopkins Hospital, Baltimore, MD.

Abstract

Background—Ablation has become an important tool in treating atrial fibrillation and ventricular tachycardia, yet the recurrence rates remain high. It is well established that ablation lines can be discontinuous, and that conduction through the gaps in ablation lines can be affected by tissue heating. In this study, we looked at the effect of tissue conductivity and propagation of electrical wavefronts across ablation lines with gaps, using both simulations and an animal model.

Methods and Results—For the simulations, we implemented a two-dimensional bidomain model of the cardiac syncytium, simulating ablation lines with gaps of varying lengths, conductivity and orientation. For the animal model, transmural ablation lines with a gap were created in 7 mongrel dogs. The gap length was progressively decreased until there was conduction block. The ablation line with a gap was then imaged using MRI, and was correlated with histology. With normal conductivity in the gap and the ablation line oriented parallel to the fiber direction, the simulation predicted that the maximum gap length that exhibited conduction block was 1.4 mm. As the conductivity was decreased, the maximum gap length with conduction block increased substantially; e.g. with a conductivity of 67% of normal, the maximum gap length with conduction block increased to 4 mm. In the canine studies, the maximum gap length that displayed conduction block acutely as measured by gross pathology correlated well (R^2 of 0.81) with that measured by MRI.

Correspondence to Ravi Ranjan, MD PhD, Division of Cardiology, University of Utah, 30 North 1900 East, Rm 4A100, Salt Lake City, Utah 84132. ravi.ranjan@hsc.utah.edu.

Disclosures There are no relevant conflict of interest disclosures for this study.

Conclusions—Conduction block can occur across discontinuous ablation lines. Moreover, with recovery of conductivity over time, ablation lines with large gaps exhibiting acute conduction block may recover propagation in the gap over time, allowing recurrences of arrhythmias. The ability to see gaps acutely using MRI will allow for targeting these sites for ablation.

Introduction

Radiofrequency ablation has become an important tool for treating atrial and ventricular arrhythmias. [1, 2] Isolation of pulmonary veins is a major component of ablation for atrial fibrillation and even though most pulmonary veins can be isolated initially, recurrences of atrial fibrillation after ablation are common, especially with persistent atrial fibrillation.[3] Numerous studies investigating the recurrence of atrial arrhythmias after the initial ablation have demonstrated that pulmonary veins that were isolated during the initial procedure do not remain isolated, and the restoration of conduction is believed to be a major factor in the recurrence of arrhythmias.[4, 5] The restoration of conduction across ablation lines has been shown to be due to gaps in the ablation line.[5] Despite attempts to create continuous transmural lesions, non-uniformity, and gaps in the ablation lines are the norm.[6] The timeline of recovery of conduction across ablation lines is quite variable, and studies have demonstrated recovery to occur as early as 20 - 60 mins after the initial ablation.[7-9] It has also been shown that when pulmonary veins are “re-isolated” after a waiting a period of 60 mins, the recurrence rate of arrhythmias over the course of a 9 month follow up is significantly reduced.[9] A better understanding of the ablation process, especially identifying and localizing the gaps in the ablation line and acting on them acutely, may significantly reduce the rate of recurrence of arrhythmias and improve the success rate of ablations.

Magnetic resonance imaging (MRI) has been used to visualize radio-frequency ablation (RFA) lesions.[10-12] RFA has also been carried out *in-vivo* under MRI guidance.[13] MRI is a powerful tool that could be used acutely to identify gaps in ablation lines, which can then be targeted to improve the success rate of ablation procedures.

In this study, we looked at the role played by these gaps in the propagation of electrical wavefronts. We first made a computational model simulating a section of (ventricular) myocardium which had ablation lines with a gap. The gap length was changed to see if conduction block developed with gaps in the line, and if so, the maximum length of the gap that failed to conduct was determined. We then changed the conductivity of the gap area itself to see if that affected the maximum gap length in the ablation line that still maintained conduction block. Finally, in an animal model, we created ablation line with gaps that had conduction block, and then acutely imaged them using MRI to see if these gaps could be visualized.

Methods

Computational Model

A 2-dimensional bidomain network model was implemented. The network model has been previously described in detail.[14, 15] For the ionic current, we used the Luo-Rudy phase I model.[16] A time step of 5 μs and a space step of 50 μm were used. The stimulating electrode was 0.25 mm by 0.25 mm in size and injected current in the extracellular domain. The programming was done using FORTRAN and the simulations were run on a Dell Desktop PC (Dell Computers, Austin, TX) with Intel Core 2 Duo Processors (Intel Corp, Santa Clara, CA). MATLAB (MathWorks, Natick, MA) was used to display the results and generate the transmembrane potential plots.

A 2-dimensional sheet measuring up to 8 mm by 8 mm was used. An ablation line of 1 mm width was implemented by decreasing the conductivity by a factor of 100 in that area. Ablation lines with varying gap lengths were simulated to determine the maximum gap length that failed to propagate the activation wavefront across the gap. Next we simulated models with the gap area having different conductivities and again the maximum gap length that had conduction block was determined. To see if the fiber orientation plays a role we made models with the ablation line oriented parallel and perpendicular to the fiber direction.

Animal Model

Institutional Animal Care and Use Committee approved the animal protocol. Seven mongrel dogs of both sexes weighing 16 to 27 kg were anesthetized with 1-2% Isoflurane and mechanically ventilated with 100% oxygen. Median-sternotomy was performed to open the chest and expose the right ventricle. We chose to make our ablation line on the right ventricle as the canine right ventricular myocardium is similar in thickness to the human atria.

Electrophysiological Measurements and Catheter Ablation

The experimental setup with ablation lines and electrode array used to measure activation pattern is shown in Figure 1. Line I is the experimental line with the gap. Activation sequence was assessed using a 5-line (A to E), 3 bipolar electrodes per line, multi-electrode array (Figure 1). The array was 20 mm × 25 mm with a separation of 5 mm between bipolar electrodes, separation of 2 mm between the bipoles of the bipolar electrodes, and a space of 9 mm between lines B and line C. The electrode array was positioned on the epicardial surface such that the linear ablation line with the gap (line I, Figure 1) fit between electrode lines B and C of the array. Bipolar pacing electrodes were placed near the atrioventricular (AV) groove on the right ventricle (RV) and the anterior wall of the left ventricle (LV).

To differentiate between slowing of conduction through the gap from conduction block, we recorded activation patterns on both sides of the gap. Once the gap became non-conductive, the activation direction recorded by the electrodes at the side farther from the pacing site reversed. To facilitate this reversal of conduction pattern after the gap became non-conducting, we created two parallel linear ablation lines (Figure 1, lines II and III). These lines (lines II and III) were created before making the experimental line (line I) and was made such that it would be perpendicular to the experimental line (line I). After creating these two parallel lines, we created the ablation line with a discontinuous segment in the middle of the line, on the right ventricular free wall (Figure 1, line I). We mapped the activation as we shortened the gap until reversal of activation pattern was observed (Figure 2).

All ablated linear lines were created using an RF generator (Atakr, Medtronic, Minneapolis, MN) and a 7 Fr. deflectable large tip standard ablation catheter (Marinr MC, Medtronic, Minneapolis, MN). Each ablation was 30-40 W applied for 60-120 seconds. The catheter was slowly moved along the epicardial surface creating a linear lesion. The epicardial gap length was measured at the narrowest non-ablated site on the epicardial surface. The gap was easily identified as pigmented tissue between the white ablated lesions.

The conduction latency between electrodes was measured at baseline and after conduction block. The conduction times is shown as median (minimum, maximum). Given that a normal distribution cannot be assumed for these measurements and the observations are paired a non-parametric, Wilcoxon signed-rank test was used for statistical significance.

Magnetic Resonance Imaging

After creating a gap with conduction block, we placed a high-resolution coil (Medrad, Indianola, PA) on the surface of the ablated myocardium. We then closed the chest and the dog was placed in the MRI scanner. All Images were acquired in a 1.5 T cardiac MRI system (Signa LX, General Electric Medical Systems, Milwaukee, WI) using the high-resolution coil, or phased array cardiac coil. Scout images were obtained using cardiac-gated fast gradient recall echo, or spoiled gradient recalled acquisition in the steady state sequence (FGRE, SPGR; TE = minimum, TR <10 msec, FA = 20, NEX = 5-10, field of view = 16 cm, slice thickness = 3 mm, 256-384 × 256 matrix, readout bandwidth = 31.25 kHz). Using the scout images, several images between the two parallel markers were acquired. We visualized the ablated lesion and detected the gap using a T2-weighted, black-blood, cardiac-gated fast spin echo (FSE) sequence (double and triple inversion recovery (IR) protocol; TR = 2 × RR, TE = 68 ms, ETL = 32, NEX = 5-10, field of view = 16 cm, slice thickness = 3 mm, 256-384 × 256 matrix, readout bandwidth = 62.5 kHz). The length of the gap was measured off-line. Some dogs were given 2-3 mg intra-venous propranolol to facilitate gating the images.

Gross and Histological Examination

After the magnetic resonance (MR) images were obtained, the dogs were euthanized with intravenous potassium chloride. The heart was removed, and after cutting the RV wall longitudinally through the experimental line, the gap length was measured. Heart tissue was fixed in 10% neutral buffered formalin. Five microtome sections were obtained from each block, and were stained with Masson's trichrome. We examined these tissues microscopically and compared the microscopic findings with the MRI findings. All data are given as median (minimum, maximum). Linear regression was used to determine the correlation between the gap length determined from tissue examination and MRI.

Results

Computational Model

The result from the model showing propagation of the activation wavefront is shown in Figure 3. The top row in Figure 3 shows snap shots of transmembrane potential in a model with no ablation line. The upper left hand corner of the model is stimulated and the wavefront propagates to cover the entire area. In the middle row of Figure 3, the model had an ablation line with a gap of 1.5 mm. Here, once again, the upper left hand corner is stimulated. After the stimulation, the wavefront reaches the ablation line and conducts through the gap to cover the entire area. In the bottom row of Figure 3, the gap was reduced to 1.3 mm. In this case the wavefront does not propagate through the gap, and the area on the other side of the ablation line is not depolarized. For these simulations the conductivity in the gap area was normal. In another set of simulations, the conductivity of the gap was reduced. Figure 4 shows the relationship between the maximum gap length that failed to conduct and fractional conductivity with the ablation line oriented parallel to the fiber direction in Figure 4A and with the ablation line oriented perpendicular to the fiber direction in Figure 4B. With the ablation line oriented parallel to the fiber direction, the maximum gap length that exhibited conduction block was 1.4 mm for normal conductivity in the gap area. As the conductivity in the gap length was reduced, there was a significant increase in the maximum gap length that had conduction block, e.g. with a conductivity of 67% of normal, the maximum gap length with conduction block increased to 4 mm. With the ablation line oriented perpendicular to the fiber direction and normal conductivity in the gap area, the maximum gap length that failed to conduct was 0.3 mm. Similar to the parallel orientation of the ablation line with fiber alignment, with the ablation line perpendicular to the fiber alignment, the maximum gap length that had conduction block increased as the conductivity

in the gap area was reduced. Also, with the ablation line oriented both parallel and perpendicular to the fiber orientation with enough reduction in conductivity there was a virtual line of block irrespective of the gap length.

Animal Model

Gap in the Ablation Line and Conduction Properties—Figure 2 shows the electrograms recorded using the bipolar array during RV (top panels) and LV (bottom panels) pacing. Prior to ablation, the median conduction latency time from electrodes A to E during RV pacing was 45 (37.5, 50) msec [median (minimum, maximum)]. During LV pacing, the median conduction latency time from E to A was 50 (42.5, 55) msec. Conduction block across the gap following ablation was recognized by reversal in activation sequence and an abrupt prolongation in conduction time. For example, during RV pacing prior to conduction block, the propagation pattern went sequentially from A to E. Once conduction block was achieved by reducing the gap length, the propagation pattern changed, and went from A to B and then to E followed by D and C. With conduction block, during RV pacing, the median conduction latency from A to C was prolonged to 92.5 (82.5, 100) msec, an increase of 105 % and during LV pacing, the median latency from E to B was prolonged to 100 (95, 115) msec, an increase of 100 %. These values were significantly longer than those at baseline (RV, $p<0.01562$; LV, $p<0.01562$ using the Wilcoxon signed-rank test).

The ablation lines and the gap were also examined anatomically. On gross examination, the ablated lesion appeared as a whitish area with a central brown region, whereas non-ablated areas retained the reddish color of muscle. Thus, the gap was easily identified as pigmented tissue between the white ablated lesions. The median length of the gap by gross examination on the epicardial surface when conduction block was established was 4.15 (1.85, 5.5) mm.

MRI Findings and Relation with Macroscopic Examination

Figure 5 shows the MR images of the ablated lesion. The left panel (Figure 5) is a slice through the RV wall perpendicular to an ablation line. In preliminary postmortem (PM) studies, we found that an ablated lesion, when imaged using FSE, usually consisted of three areas; i.e. an inner area with low intensity, a middle area with intermediate intensity, and an outer area with low intensity as seen in this figure as well. The right panel in Figure 5 is a section parallel to an ablation line with a gap in the middle. We defined the gap length as the distance between the outer low intensity areas. Figure 6 shows a gross pathology specimen with the ablation line and correlating MR image with the areas delineated. The median gap length determined using MRI was 4.15 (1.65, 6.5) mm. Gap length measured by macroscopic examination correlated well with that measured using MRI with a correlation coefficient (R^2) of 0.81.

Histological Examination and Relation with Results of MRI

On Masson's trichrome stain, the ablated areas appeared as a well circumscribed blue-staining area of necrosis surrounded by normal myocardium (Figure 7). The gap between the ablated areas also stains red on Masson's trichrome stain indicating that this area was not ablated. The ablated area corresponding to coagulation necrosis showed eosinophilic myocardial fibers with pyknosis. Disruption of the architecture of myocardial fibers was often seen in the center of the blue area, while the peripheral blue area had relatively preserved dense tissue. Contraction band necrosis was noted in the border zone between the ablated area and normal myocardium, surrounding a region of coagulation necrosis. No marked hemorrhage or hematoma was detected in the ablated lesion. We compared the histological findings with the three areas of varying intensities as seen in MRI as shown in Figure 6. From the center of ablated area going towards normal tissue, the three layers

corresponded to coagulation necrosis with severe myocardial damage, coagulation necrosis with mild myocardial damage, and contraction band necrosis.

Discussion

The recurrence of arrhythmias after ablation is common and frequently leads to repeat procedures.[3] In cases of atrial fibrillation many of these recurrences are due to restoration of electrical connections to previously isolated pulmonary veins.[5, 17] In this study, we explored the possibility that gaps present in the ablation lines are a cause of acute success but eventual restoration of electrical connectivity leading to recurrence of arrhythmias. We also explored using MRI as an imaging tool to visualize these gaps acutely so that they could be targeted for better outcomes.

Both our simulation (Figures 3 and 4) and experimental (Figure 2) results show that there can be gaps in ablation lines that nonetheless produce conduction block. Moreover, the relationship between the gap length and the development of conduction block is dependent on the conductivity of the tissue. A reduction in tissue conductivity allows for larger gaps that do not conduct (Figure 4). Our modeling results are consistent with prior one-dimensional model reported by Cabo et. al. [18] in that the block happens after passing through the higher resistance in the gap area.

It has previously been shown that heating the tissue during RF ablation acutely affects the cellular electrophysiological properties and the response to heating is graded depending both on the tissue temperature and also the distance from the site of ablation.[19-21] Prior studies have also shown that this acute graded change in the electrophysiological properties with distance from the ablation site recovers right up to the boundary of tissue destruction.[21] Wood et. al.[21] found that after RF ablation, acute measurements of action potential duration shows a gradual progression to normal over a distance of about 3.5 mm from the boundary of the ablated area, but chronically, over the course of one to four weeks the tissue recovers and the action potential is normal in myocardium at the boundary of the ablated area. In another acute study done in canine ventricular wedge preparations there was a marked decrease in conduction velocity and dV/dt for temperatures above 45° C.[22] Simmers et. al. also using a canine myocardial wedge preparation showed that there was transient conduction block for temperature ranging from 45° C to 55° C when the wedge was heated for 30 seconds.[23] We therefore postulate, that due to tissue heating, the electrophysiological properties change acutely, allowing for larger gaps that have conduction block, but as the tissue recovers, the gap that was non-conducting acutely may become conductive. In our animal experiments the median maximum gap length that exhibited acute conduction block was 4.15 mm which was significantly larger than the 1.4 mm predicted by the simulation for normal conduction in the gap area. In theory, any gap greater than 1.4 mm which caused acute conduction block with recovery, could conduct again leading to recurrence of arrhythmias.

We also showed that these gaps can be visualized acutely using MRI (Figure 5 and 6). Moreover the gap length as measured by MRI correlated well with that measured using histology. MRI has been used to characterize ablated areas[10, 11] and see ablation lesions in real time before [12], but has not been employed for gap detection. In prior studies, the extent of left atrial scarring as quantified by MRI has been correlated with procedural outcomes,[24] but targeting a specific gap area could be very useful in improving the outcome and limiting the amount of scar.

Limitations

We did not measure tissue conductivity directly in the animal model, so we cannot be certain about the degree to which the decrease in conduction played a role in determining the gap length that produced conduction block. A direct measurement of conductivity is difficult as the volume of the gap tissue is much smaller than the myocardium around it and as a result any measurement in the intact heart will reflect the overall conductivity than just that of the gap area itself. In addition, we did not determine if there was reversal of conduction block over time in the animal model. Such latter measurements would require doing chronic animal experiments which was beyond the scope of these studies.

Conclusion

In conclusion we have shown that conduction block is possible across ablation lines with a gap. The model predicts that the maximum length of the gap that results in conduction block depends on the conductivity of the tissue. Since the conductivity of the tissue is dependent on the electrophysiological properties which are affected by the temperature to which the tissue is heated to, we propose that gaps that are acutely non-conducting allow conduction at a later time as the tissue recovers, leading to restoration of electrical conductivity across ablation lines. We have also shown that these gaps can be visualized using MRI which can be very helpful in the future in targeting these lesions for improved long term success of the procedure.

Supplementary Material

Refer to Web version on PubMed Central for supplementary material.

Acknowledgments

The study was funded by National Institutes of Health Grants: RO1-HL64795 and R01-HL094610 to Dr. Halperin, and a grant from the Donald W. Reynolds Foundation.

References

1. Haissaguerre M, Jais P, Shah DC, Takahashi A, Hocini M, Quiniou G, Garrigue S, Le Mouroux A, Le Metayer P, Clementy J. Spontaneous initiation of atrial fibrillation by ectopic beats originating in the pulmonary veins. N Engl J Med. 1998; 339:659–66. [PubMed: 9725923]
2. d′Avila A, Ruskin JN. Nonpharmacologic strategies: the evolving story of ablation and hybrid therapy. Am J Cardiol. 2008; 102:20H–24H.
3. Fisher JD, Spinelli MA, Mookherjee D, Krumerman AK, Palma EC. Atrial fibrillation ablation: reaching the mainstream. Pacing Clin Electrophysiol. 2006; 29:523–37. [PubMed: 16689850]
4. Cappato R, Negroni S, Pecora D, Bentivegna S, Lupo PP, Carolei A, Esposito C, Furlanello F, De Ambroggi L. Prospective assessment of late conduction recurrence across radiofrequency lesions producing electrical disconnection at the pulmonary vein ostium in patients with atrial fibrillation. Circulation. 2003; 108:1599–604. [PubMed: 12963643]
5. Ouyang F, Antz M, Ernst S, Hachiya H, Mavrakis H, Deger FT, Schaumann A, Chun J, Falk P, Hennig D, Liu X, Bansch D, Kuck KH. Recovered pulmonary vein conduction as a dominant factor for recurrent atrial tachyarrhythmias after complete circular isolation of the pulmonary veins: lessons from double Lasso technique. Circulation. 2005; 111:127–35. [PubMed: 15623542]
6. Jumrussirikul P, Atiga WL, Lardo AC, Berger RD, Halperin H, Hutchins GM, Calkins H. Prospective comparison of lesions created using a multipolar microcatheter ablation system with those created using a pullback approach with standard radiofrequency ablation in the canine atrium. Pacing Clin Electrophysiol. 2000; 23:203–13. [PubMed: 10709228]

7. Sauer WH, McKernan ML, Lin D, Gerstenfeld EP, Callans DJ, Marchlinski FE. Clinical predictors and outcomes associated with acute return of pulmonary vein conduction during pulmonary vein isolation for treatment of atrial fibrillation. Heart Rhythm. 2006; 3:1024–8. [PubMed: 16945795]
8. Cheema A, Dong J, Dalal D, Marine JE, Henrikson CA, Spragg D, Cheng A, Nazarian S, et al. Incidence and time course of early recovery of pulmonary vein conduction after catheter ablation of atrial fibrillation. J Cardiovasc Electrophysiol. 2007; 18:387–91. [PubMed: 17394453]
9. Wang XH, Liu X, Sun YM, Gu JN, Shi HF, Zhou L, Hu W. Early identification and treatment of PV re-connections: role of observation time and impact on clinical results of atrial fibrillation ablation. Europace. 2007; 9:481–6. [PubMed: 17522081]
10. Dickfeld T, Kato R, Zviman M, Lai S, Meininger G, Lardo AC, Roguin A, Blumke D, Berger R, Calkins H, Halperin H. Characterization of radiofrequency ablation lesions with gadolinium-enhanced cardiovascular magnetic resonance imaging. J Am Coll Cardiol. 2006; 47:370–8. [PubMed: 16412863]
11. Dickfeld T, Kato R, Zviman M, Nazarian S, Dong J, Ashikaga H, Lardo AC, Berger RD, Calkins H, Halperin H. Characterization of acute and subacute radiofrequency ablation lesions with nonenhanced magnetic resonance imaging. Heart Rhythm. 2007; 4:208–14. [PubMed: 17275759]
12. Vergara GR, Vijayakumar S, Kholmovski EG, Blauer JJ, Guttman MA, Gloschat C, Payne G, Vij K, Akoum NW, Daccarett M, McGann CJ, Macleod RS, Marrouche NF. Real-time magnetic resonance imaging-guided radiofrequency atrial ablation and visualization of lesion formation at 3 Tesla. Heart Rhythm. 2010
13. Lardo AC, McVeigh ER, Jumrussirikul P, Berger RD, Calkins H, Lima J, Halperin HR. Visualization and temporal/spatial characterization of cardiac radiofrequency ablation lesions using magnetic resonance imaging. Circulation. 2000; 102:698–705. [PubMed: 10931812]
14. Ranjan, R. *Mechanism of anodal stimulation in cardiac tissue* in *Biomedical Engineering (PhD Thesis)*. The Johns Hopkins University; Baltimore, MD: 1997.
15. Ranjan R, Tomaselli GF, Marban E. A novel mechanism of anode-break stimulation predicted by bidomain modeling. Circ Res. 1999; 84:153–6. [PubMed: 9933246]
16. Luo CH, Rudy Y. A model of the ventricular cardiac action potential. Depolarization, repolarization, and their interaction. Circ Res. 1991; 68:1501–26. [PubMed: 1709839]
17. Haissaguerre M, Hocini M, Sanders P, Sacher F, Rotter M, Takahashi Y, Rostock T, Hsu LF, Bordachar P, Reuter S, Roudaut R, Clementy J, Jais P. Catheter ablation of long-lasting persistent atrial fibrillation: clinical outcome and mechanisms of subsequent arrhythmias. J Cardiovasc Electrophysiol. 2005; 16:1138–47. [PubMed: 16302893]
18. Cabo C, Barr RC. Unidirectional block in a computer model of partially coupled segments of cardiac Purkinje tissue. Ann Biomed Eng. 1993; 21:633–44. [PubMed: 8116915]
19. Nath S, Lynch C 3rd, Whayne JG, Haines DE. Cellular electrophysiological effects of hyperthermia on isolated guinea pig papillary muscle. Implications for catheter ablation. Circulation. 1993; 88:1826–31. [PubMed: 8403328]
20. Nath S, Redick JA, Whayne JG, Haines DE. Ultrastructural observations in the myocardium beyond the region of acute coagulation necrosis following radiofrequency catheter ablation. J Cardiovasc Electrophysiol. 1994; 5:838–45. [PubMed: 7874329]
21. Wood MA, Fuller IA. Acute and chronic electrophysiologic changes surrounding radiofrequency lesions. J Cardiovasc Electrophysiol. 2002; 13:56–61. [PubMed: 11843484]
22. Simmers TA, De Bakker JM, Wittkampf FH, Hauer RN. Effects of heating on impulse propagation in superfused canine myocardium. J Am Coll Cardiol. 1995; 25:1457–64. [PubMed: 7722149]
23. Simmers TA, de Bakker JM, Wittkampf FH, Hauer RN. Effects of heating with radiofrequency power on myocardial impulse conduction: is radiofrequency ablation exclusively thermally mediated? J Cardiovasc Electrophysiol. 1996; 7:243–7. [PubMed: 8867298]
24. McGann CJ, Kholmovski EG, Oakes RS, Blauer JJ, Daccarett M, Segerson N, Airey KJ, Akoum N, Fish E, Badger TJ, DiBella EV, Parker D, MacLeod RS, Marrouche NF. New magnetic resonance imaging-based method for defining the extent of left atrial wall injury after the ablation of atrial fibrillation. J Am Coll Cardiol. 2008; 52:1263–71. [PubMed: 18926331]

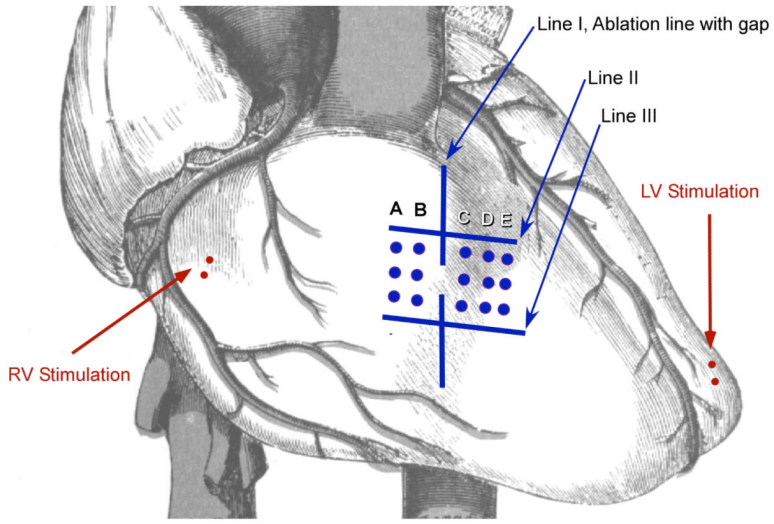

Figure 1.
Experimental set-up. Line I: Experimental ablation line with a gap. The gap length was decreased until there was no conduction across the gap. Line II and III: These are ablation lines created prior to Line I and oriented perpendicularly to the experimental line (line I). An electrode array with bipoles (columns A to E) was used to record local electrograms.

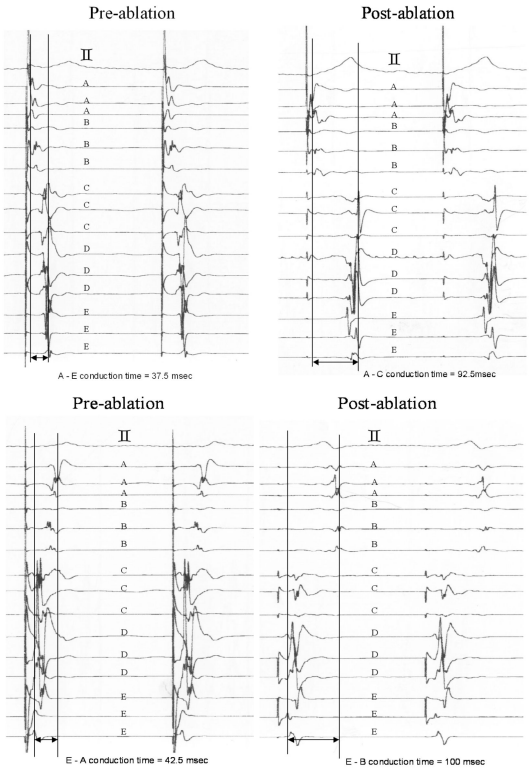

Figure 2.

Electrograms (EGMs) before and after creation of conduction block across the gap. Letters A to E indicate the electrode column from which the EGMs were recorded. The top tracing is an ECG lead. The left panels show the EGMs before conduction block and the right panels are after conduction block. The top panels were recorded during RV pacing, close to the AV groove. The bottom panels were recorded during LV pacing at the apex. During RV pacing (top left panel) the activation goes sequentially from A to E. After conduction block is achieved (top right panel) the sequence changes and the activation goes from A to B and then after significant delay is recorded at E and then at D and finally at C. Similarly, with LV pacing the sequence changes after conduction block.

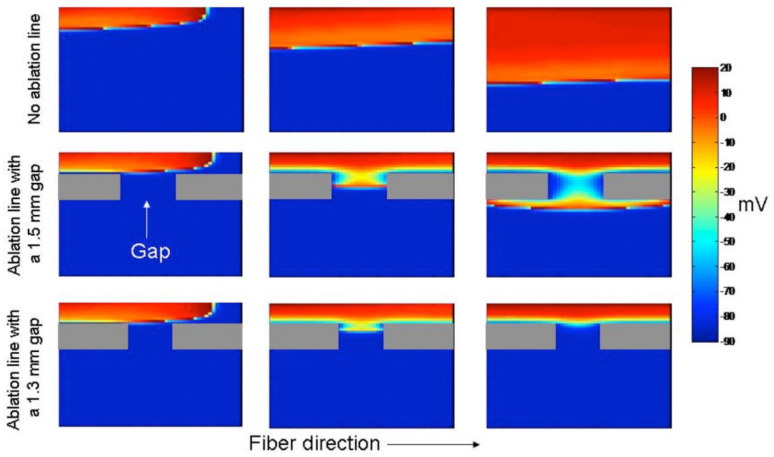

Figure 3.

Computational model result showing snapshots of transmembrane potential across simulated myocardial tissue. For these models a 5 mm by 5 mm plane of tissue was simulated. Each row represents a different model and the panels in a row show snapshots as time progresses going from left to right. With no ablation line (top row) the depolarization spreads to cover the entire tissue. With an ablation line and a 1.5 mm gap of normal conductivity the depolarization propagates through the gap to cover the entire area. With an ablation line and a 1.3 mm gap of normal conductivity the depolarization does not propagate through the gap area resulting in conduction block.

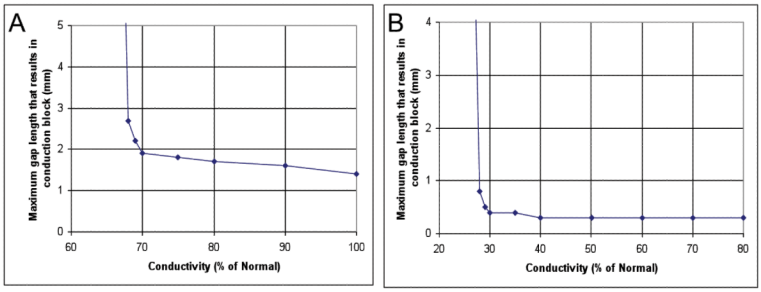

Figure 4.

A plot of the maximum gap length that results in conduction block versus conductivity (normalized to 100%) in the gap area. Panel **A** is with the ablation line oriented parallel to the fiber direction. Panel **B** is with the ablation line oriented perpendicular to the fiber.

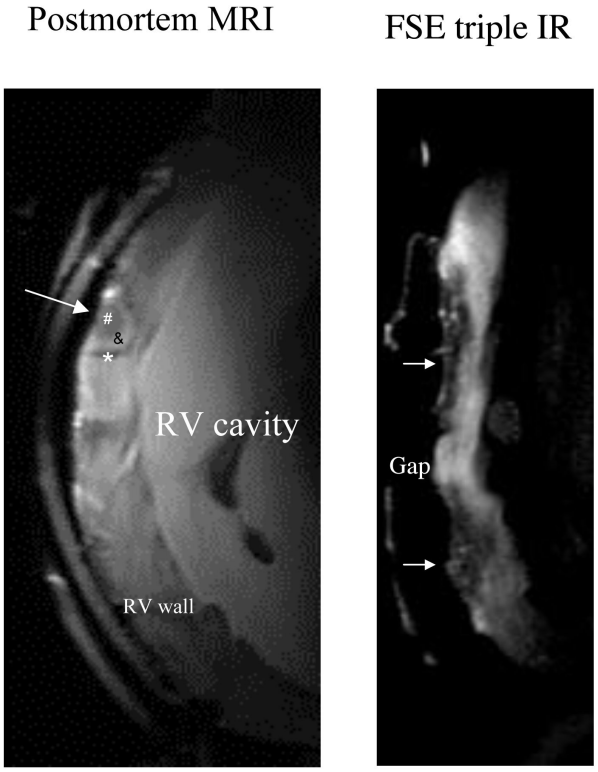

Figure 5.
MRI images of the ablation line. The image on the left was taken using a non-cardiac gating FSE sequence. This is a cross-sectional view (perpendicular to the ablation line) of the ablated lesion (arrow) with three distinct areas. There is an inner area with low intensity (#), middle area with intermediate intensity (&) and an outer rim area with low intensity (*). The image on the right is a section along the length of a linear ablation line with gap taken using a T2-weighted Triple IR FSE sequence. The ablated areas are dark (arrows) and the gap in the middle is bright in appearance.

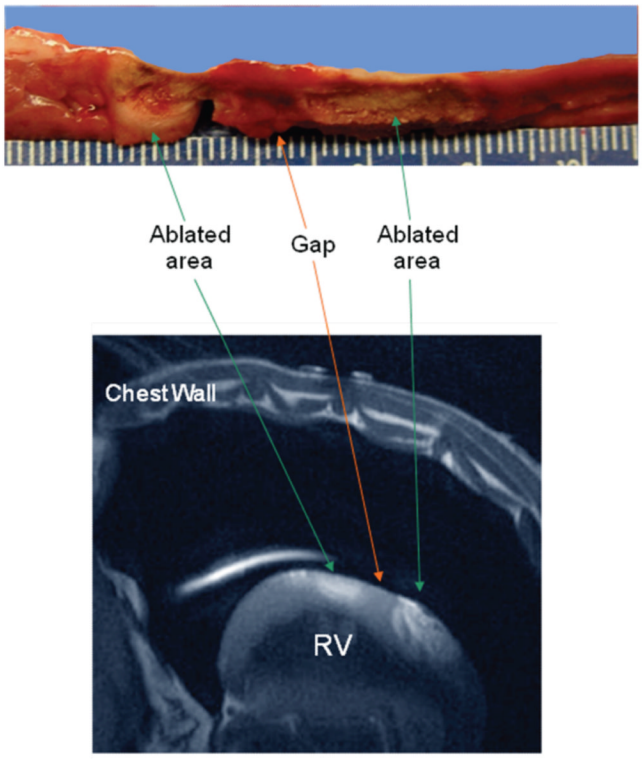

Figure 6.
Macroscopic section and MR image of the ablation line. The top panel shows a gross specimen with a longitudinal section cut along the ablation line. In the middle of the ablation line is the non-conducting gap. The bottom panel is an MR image of an ablation line with gap.

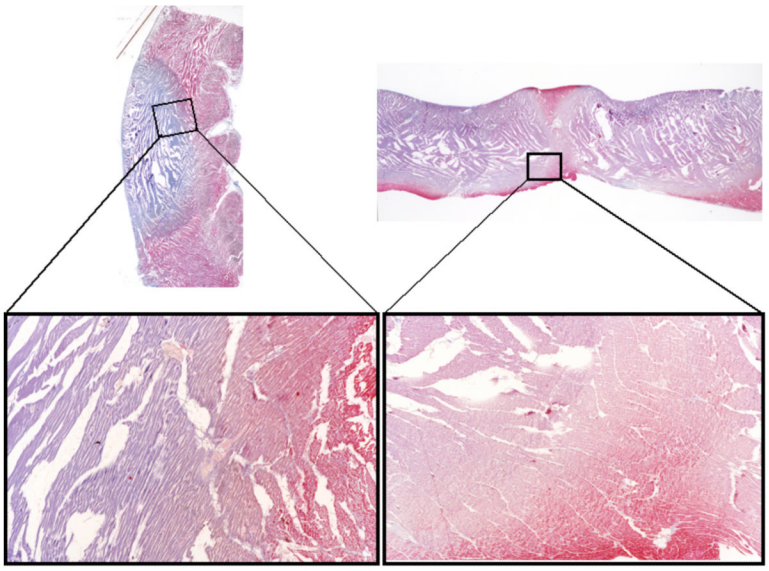

Figure 7.

Masson's trichrome stain of tissue with linear ablations. The left and right panels are from two different specimens. The bottom panels show magnified image of a small area. The ablated area appears as blue and normal myocardium as red. On high magnification (X16), three different areas are noted: inner area of severely damaged coagulation necrosis, middle area of mild damaged coagulation necrosis, and an outermost area of contraction band necrosis.